Applied Surface Science 754 (2027) 168516

Contents lists available at ScienceDirect

Applied Surface Science

journal homepage: www.elsevier.com/locate/apsusc

Full Length Article

Grafting-density-controlled superhydrophilic chitosan-graft-poly(carboxybetaine methacrylate) coatings for protein-resistant biointerfaces

Theodore Sentoukas [a,*], Andrzej Marcinkowski [a], Wojciech Wałach [a], Karolina Olszowska [a], Aristeidis Papagiannopoulos [b], Stergios Pispas [b], Barbara Trzebicka [a]

[a] Centre of Polymer and Carbon Materials, Polish Academy of Sciences, ul. M. Curie-Skłodowskiej 34, 41-819 Zabrze, Poland
[b] Institute of Theoretical and Physical Chemistry, National Hellenic Research Foundation, 48 Vassileos Constantinou Ave., GR11635 Athens, Greece

ARTICLE INFO

Keywords:
Chitosan
PCBMA
Super hydrophilic polymers
Thin-films
Antifouling biointerfaces

ABSTRACT

Chitosan is a renewable and chemically versatile biopolymer, but its use in fouling-prone environments is limited by its tendency to interact with proteins and other biological species. In this work, chains of superhydrophilic zwitterionic poly(carboxybetaine methacrylate) (PCBMA) were grafted onto chitosan to improve its surface hydration and protein resistance. PCBMA homopolymers with different molar masses were synthesized by RAFT polymerization and then grafted onto chitosan using a grafting-to approach. The grafting behavior depended strongly on PCBMA chain length: shorter PCBMA chains led to higher grafting density, while longer chains resulted in lower substitution because of increased steric limitations. CS and CS-g-PCBMA copolymers were then deposited as thin films on silicon oxide wafers by spin coating to evaluate surface morphology, wettability, and protein fouling. The retention of protein was studied with bovine serum albumin (BSA) as model protein. This study showed that length and grafting density of PCBMA control the surface properties of CS-g-PCBMA thin films. Thin films produced from densely grafted CS with short PCBMA chains led to smooth, highly wettable, and protein-resistant chitosan-based coatings. These findings provide a useful strategy for designing hydrated, polysaccharide-based zwitterionic surfaces for antifouling applications.

1. Introduction

Chitosan has attracted attention as a versatile and renewable biopolymer, widely employed in drug and gene delivery [1–3], vaccine adjuvants [4], antibacterial wound dressings [5,6] and tissue engineering scaffolds [7]. Beyond medicine, chitosan has also been explored in dye and heavy metal removal [8], antimicrobial coatings and food packaging membranes [9,10]. Chitosan's biodegradability, biocompatibility, and chemical reactivity, arising from its amino and hydroxyl groups, make it a promising building block for functional materials [11]. Native chitosan exhibits limited chemical stability and poor resistance to nonspecific adsorption of biomolecules, cells, and microorganisms, which restricts its performance in hydration-intensive or fouling-prone environments.

Chemical modification has become a key strategy to tailor chitosan's properties by improving solubility, charge distribution, and interfacial behavior [12,13]. Controlled polymerization techniques, such as reversible addition–fragmentation chain-transfer (RAFT) and atom-transfer radical polymerization (ATRP), allow tunable graft length and density. For example, thermoresponsive PMEO2MA [14], PAA [15], and PNIPAAm [16,17] chains have been introduced onto chitosan, while ATRP-based approaches have been used to prepare PHEMA-containing chitosan surfaces [18]. Sun et al. [19] grafted PCBMA brushes from chitosan nanofibers and demonstrated reduced nonspecific cell adhesion, confirming the potential of combining chitosan with carboxybetaine chemistry. Nevertheless, the effect of systematically varying the architecture of preformed PCBMA grafts, particularly the relationship between PCBMA chain length, resulting grafting density, and the surface properties of planar chitosan-based coatings, has received much less attention.

Resistance to nonspecific protein adsorption is associated with the formation of a stable and highly hydrated interfacial layer that can reduce direct contact between proteins and the underlying surface [20,21]. Zwitterionic polymers contain oppositely charged groups

* Corresponding author.
E-mail address: tsentoukas@cmpw-pan.pl (T. Sentoukas).

https://doi.org/10.1016/j.apsusc.2026.168516
Received 13 July 2026; Received in revised form 15 September 2026; Accepted 25 September 2026
Available online 3 October 2026
0169-4332/© 2026 The Author(s). Published by Elsevier B.V. This is an open access article under the CC BY license (http://creativecommons.org/licenses/by/4.0/).

within the same repeat unit that can strongly bond with water via electrostatic interactions while remaining overall electrically neutral [22]. Among these materials, poly(carboxybetaine methacrylate) (PCBMA) is a zwitterionic polymer known for its excellent antifouling performance [23,24], strong hydration capability [25,26] and biocompatibility [27,28]. PCBMA has also demonstrated reduced immune response and prolonged circulation time in comparison to PEG analogues in certain systems [29].

The antifouling performance of a zwitterionic layer is expected to depend on its macromolecular architecture. Parameters such as density and side-chain length can influence the amount of zwitterionic material present at the interface, steric effects between neighboring chains, chain accessibility, surface morphology, and the ability of the coating to maintain a hydrated interfacial environment [30,31]. Understanding the interplay between these parameters is important for designing chitosan-based coatings in which the beneficial properties of the polysaccharide are combined with efficient resistance to protein fouling.

In this study, chitosan-graft-poly(carboxybetaine methacrylate) (CS-g-PCBMA) copolymers were synthesized via a RAFT-mediated grafting-to approach using PCBMA chains of different molar masses. The resulting graft copolymers were deposited through spin-coating as thin-film coatings on silicon oxide wafers to evaluate how PCBMA chain length and grafting density affect surface morphology, wettability, and protein retention. The CS-g-PCBMA copolymers were molecularly characterized by 1H NMR to determine composition, grafting density and degree of substitution. The deposited films were characterized by AFM, contact angle measurements, and BSA retention assay. This work aimed to establish a direct connection between the relationship among composition, grafting density, surface wettability, and antifouling properties for zwitterionic chitosan-based coatings. The results demonstrate that dense grafting with short PCBMA chains produces smooth, highly wettable, and protein-resistant thin films, providing a simple route toward renewable polysaccharide-based antifouling biointerfaces.

2. Materials

Chitosan (M_n = 164 kDa, degree of deacetylation ≈ 90%), β-propiolactone (Grade II, ≥90%), 4,4′-azobis(4-cyanovaleric acid) (ACVA; ≥98.0%), 4-cyano-4-(phenylcarbonothioylthio)pentanoic acid (CPADB), bovine serum albumin (BSA; monomer ≥97%, assay ≥97% by PAGE) were purchased from Sigma-Aldrich and used as received. Ethanol (absolute, ≥99.8%, analytical reagent grade) and acetic acid (Glacial, Certified ACS) were purchased from Fisher Chemical. 2-(Dimethylamino)ethyl methacrylate (DMAEMA; 98%), was purchased from Sigma-Aldrich and purified by distillation before use. Water was purified using a commercial Hydrolab (Staszyn, Poland) ion-exchange system and was used for polymerization, dialysis, and aqueous solution preparation.

3. Methods

3.1. Synthesis

3.1.1. Synthesis of CBMA

The synthesis of CBMA monomer was performed following a method by Liaw et al. [32]. Briefly, DMAEMA was reacted with β-propiolactone in dry acetone under argon, followed by filtration, washing with dry acetone, and drying. A detailed synthesis and purification procedure is provided in the Supporting Information and shown schematically in Fig. S1.

3.1.2. Synthesis of PCBMA

Three PCBMA homopolymers were synthesized via RAFT polymerization. For synthesis of $PCBMA_{40}$, 4-cyano-4-(phenylcarbonothioylthio) pentanoic acid dithioester benzoate (CPADB) (0.0144 g, 0.0515 mmol) was used as RAFT CTA and 4,4′-azobis(4-cyanovaleric acid) (ACVA) (0.0036 g, 0.0129 mmol) as radical initiator. Both were solubilized in 3 mL of ethanol. CBMA (0.5 g, 2.18 mmol) was solubilized in 3 mL of deionized water. Both solutions were mixed in a round glass flask followed by 20-minute degassing using argon gas. The mixture was then placed in an oil bath at 70 °C for 8 h. The reaction was terminated via quenching in liquid nitrogen and exposure to air. The reaction solution was subjected to a 3-day dialysis in water using a 1000 Da M_n cut-off dialysis bag.

The conditions for $PCBMA_{23}$ and $PCBMA_6$ synthesis are described in SI.

3.1.3. Synthesis of CS-g-PCBMA

Synthesized PCBMAs were further used for grafting onto chitosan. PCBMA (0.2 g), chitosan (0.2 g) and ACVA were solubilized in water with 4 vol% acetic acid, purged in argon for 20 min and left to react for 24 h at 70 °C. PCBMA/ACVA molar ratio was set to 4:1. Accordingly, 1.52 mg (0.00543 mmol), 2.70 mg (0.00962 mmol), and 9.34 mg (0.0333 mmol) of ACVA were used for $PCBMA_{40}$, $PCBMA_{23}$, and $PCBMA_6$, respectively. The reaction mixtures were dialyzed for 5 days in deionized water. Three CS-g-PCBMA copolymers were obtained and the final products were isolated via lyophilization.

3.2. Degree of substitution and grafting yield calculations

The composition of CS-g-PCBMA copolymers was determined from ^{1}H NMR spectra from characteristic peak integrals assigned to the chitosan backbone (denoted as j at 3.05 ppm in Fig. S6) and PCBMA grafts (denoted as f at ~2.9 ppm, as shown in Fig. S6). The mass fractions of chitosan and PCBMA in the copolymer are denoted as W_{CS} and W_{PCBMA}, respectively. The average number of PCBMA chains per chitosan chain was calculated according to:

$$N_{PCBMAchainsperCSchain} = \frac{w_{PCBMA}/M_{n,PCBMA}}{w_{CS}/M_{n,CS}} \quad (1)$$

where $M_{n,PCBMA}$ is the number-average molar mass of the PCBMA precursor and $M_{n,CS}$ is the number-average molar mass of chitosan.

The number of CS-repeat units per chain was estimated from the nominal chitosan molar mass and the average repeat-unit molar mass. The latter was calculated from the degree of deacetylation (DD), taking into account the relative fractions of deacetylated D-glucosamine units (GlcN) and residual N-acetyl-D-glucosamine units (GlcNAc):

$$M_{CSunit} = DD \times M_{GlcN} + (1 - DD) \times M_{GlcNAc} \quad (2)$$

$$N_{CSunitsperchain} = \frac{M_{n,CS}}{M_{CS,unit}} \quad (3)$$

where M_{GlcN} and M_{GlcNAc} are the molar masses of the deacetylated glucosamine and acetylated N-acetylglucosamine repeat units, respectively, and DD is expressed as a fraction.

The degree of substitution, DS, was defined as the percentage of chitosan repeat units bearing one PCBMA graft:

$$DS(\%) = \frac{N_{PCBMAgraftsperCSchain}}{N_{CSunitsperchain}} \times 100 \quad (4)$$

The grafting yield (GY) was defined in this work as the molar percentage of grafted CBMA repeat units relative to chitosan repeat units:

$$GY(\%) = \frac{N_{PCBMAgraftsperCSchain} \times DP_{PCBMA}}{N_{CSunitsperchain}} \times 100 \quad (5)$$

where DP_{PCBMA} the degree of polymerization is given from:

$$DP_{PCBMA} = \frac{M_{n,PCBMA}}{M_{CBMA}} \quad (6)$$

3.3. Thin-film preparation

Model thin-film coatings were prepared by spin coating of CS and CS-g-PCBMA solutions onto silicon oxide wafers cut into approximately 1 cm × 1 cm pieces. Before coating, the wafers were cleaned sequentially with ethanol, deionized water and acetone, dried under an argon stream, and plasma-cleaned for 10 min at 20–25% generator power, immediately before deposition. CS and CS-g-PCBMA samples were dissolved in deionized water containing 4 vol% acetic acid at concentrations of 5 and 10 mg mL^{-1} and stirred until complete dissolution. For each film, 100 μL of polymer solution was deposited onto the cleaned wafer surface and spin-coated using a two-step program: 300 rpm for 30 s, followed by 2000 rpm for 120 s. Pure chitosan films were prepared by the same procedure and used as reference coatings. The samples were studied to evaluate the influence of CS-g-PCBMA composition and film thickness on surface morphology, wettability, and short-term protein retention under identical preparation conditions.

3.4. Protein antifouling assay

Protein retention on CS and CS-g-PCBMA coatings was evaluated using bovine serum albumin (BSA) as a model protein. The assay was adapted from established adsorption/desorption approaches used to study protein adsorption on solid surfaces [33,34]. Film-coated silicon oxide wafers with an exposed surface area of approximately 1.0 cm^2 were immersed in 1 mL of BSA solution prepared in deionized water at a concentration of 2 mg/mL and incubated at 37 °C for 1 h. The BSA solution pH was 7.5, checked before and after the assay. Under these conditions, each film was exposed to a total BSA amount of 2 mg. After incubation, the films were gently rinsed with deionized water to remove loosely associated protein.

Protein retained by the coatings was recovered by immersing each coated wafer in 1 mL of 6 M urea solution for 1 h. Then, the resulting desorption solutions were analyzed by UV–Vis spectroscopy at 218 nm using a 1 cm optical path length. Urea-only blanks and film-plus-urea blanks without prior BSA exposure were measured and subtracted from the corresponding sample absorbance values to account for background contributions from the desorption medium and possible coating-derived signals.

The BSA concentration in the desorption solution was determined using Beer-Lambert's law:

$$A_{abs} = \varepsilon c l \tag{7}$$

where Aabs is the absorbance at 218 nm, ε is the extinction coefficient of BSA in 6 M urea (6.7 mL $mg^{-1}cm^{-1}$), c is the BSA concentration (mg mL^{-1}), and l is the optical path length (1 cm).

The amount of retained BSA was calculated as:

$$\Gamma_{BSA} = \frac{cV}{A_s} \tag{8}$$

where Γ_{BSA} is the amount of retained BSA normalized to the exposed coating area, V is the volume of the urea desorption solution, and A_s is the exposed film area. Values were expressed as μg/cm^2. For each sample, one desorption solution obtained from the BSA-retention assay was analyzed three times by UV–Vis spectroscopy. The reported value represents the mean of the three instrumental measurements. Values indistinguishable from the corresponding blanks were reported as below the detection limit. The reported values represent the total BSA recovered from the coatings after urea treatment and may include both surface-associated protein and protein taken up within the hydrated polymer film.

3.5. Measurements

Molar mass measurements of PCBMA homopolymers were performed by size exclusion chromatography (SEC-MALS). SEC system comprised of a 1260 Agilent Technologies isocratic pump, column oven Knauer, multi-angle light scattering detector (λ = 690 nm) DAWN EOS (Wyatt Technologies), Dn-2010 RI refractometer detector (WGE Dr. Bures), Waters column Ultrahydrogel 250, 7.8 x 300 mm and the guard column Ultrahydrogel 6 × 40 mm. Measurements were carried out in 0.2 M $NaNO_3$ water solution, at a temperature of 35 °C, at eluent flow of 0.5 mL/min. ASTRA 4 software (Wyatt Technologies) was used for recording data and performing calculations using dn/dc value of PCBMA (0.147 mL/g) measured in the lab.

The refractive index increment (dn/dc), necessary to calculate the actual mass of PCBMA homopolymers, was determined using the SEC-3010 dn/dc refractometer detector at a wavelength of λ = 620 nm. The measurement was made for five concentrations in 0.2 M $NaNO_3$ water solution, ranging from 0.5 g/L to 7 g/L, at a temperature of 35 °C. At least three measurements were made for each concentration. BI-DNDCW software was used to record data and perform calculations.

Spectra of CS, PCBMA and CS-g-PCBMA were obtained using an FT-IR 6700 spectrometer (Nicolet, Thermo Scientific) equipped with a diamond-crystal Smart Orbit™ accessory operating in attenuated total reflection (ATR) mode. All spectra were acquired over the range of 500–4000 cm^{-1} with 64 accumulations.

The ^1H NMR spectra of all samples were recorded on a Bruker® Ultrashield 600 Plus spectrometer (Billerica, MA, USA) operating at 600 MHz in D_2O, containing 4 vol% acetic acid, with sodium 4,4-dimethyl-4-silapentane-1-sulfonate-d_6 (DSS-d_6) as the reference.

AFM measurements were conducted using a Dimension ICON AFM microscope equipped with a NanoScope V controller (BRUKER Corporation, Santa Barbara, CA, US) operating in a soft tapping mode in air, utilizing a standard 125 μm long and 10 - 15 μm high tip and a single-crystal doped silicon cantilever with a flexural stiffness of 10 - 130 N m^{-1} (Model PPP-NCH 10, NANOSENSORS, Neuchatel, Switzerland). Images were obtained with a piezoelectric scanner having a nominal size of 85 μm × 85 μm size and recorded using NanoScope Analysis 1.9 Software (BRUKER Corporation, Santa Barbara, CA, US), with the most representative images selected from three measurements taken on multiple samples. The approximate thickness of the polymer film was determined by scratching the polymer layer on the surface using the same AFM tip in contact mode over a 1 × 2 μm area. The scratched region was then imaged in tapping mode over a 5 × 5 μm area. The approximate CS and CS-g-PCBMA thin-films thickness was estimated from a single topographical cross-section measured across the scratched region.

Static contact angle measurements (θ) of the modified surfaces were performed using a CAM101 contact angle goniometer (KSV Instruments) equipped with a temperature-control unit, an intelligent digital controller OMRON 5EGN with an accuracy of ±1 °C, connected to a thermostatically controlled chamber. Water contact angles were measured in air using the sessile-drop method. A series of images of a water droplet, approximately 3 μL, was collected over 30 s, and the average contact angle was calculated. Three independently prepared films were analyzed for each coating condition with three droplets measured at different positions on each film. The mean contact angle for each film was calculated from the three droplet measurements and the results are reported as the mean ± standard deviation of three independently prepared films (n = 3).

Scanning electron microscopy (SEM) studies of CS, CS-g-$PCBMA_{23}$ and CS-g-$PCBMA_6$ were performed using a Quanta 250 FEG (FEI/Thermo Fisher Scientific) device, using low-vacuum techniques at accelerating voltages ranging from 5.0 to 15.0 kV.

4. Results and discussion

4.1. Synthesis and molecular characterization

Three PCBMA homopolymers with different molar masses were

synthesized for subsequent grafting onto CS backbone. PCBMA was prepared via RAFT polymerization using CPADB as RAFT CTA and ACVA radical initiator in water/ethanol mixture, as shown in Fig. S2. This synthetic route is based on previous experiments in the laboratory for CBMA monomer. ^{1}H NMR spectra of all PCBMA homopolymers are presented in Fig. S3. ^{1}H NMR spectrum of pristine CS is presented in Fig. S4. Molar masses of the PCBMA samples were 9200 Da (DP = 40), 5200 Da (DP = 23) and 1500 Da (DP = 6), measured by SEC-MALS in water, using dn/dc of PCBMA (0.147 mL/g), as shown in Fig. S5. The corresponding data for the synthesized polymers and their graft copolymers are summarized in Table 1.

PCBMA homopolymers of different lengths were used to prepare grafted chitosan, allowing the effect of grafted chain length to be examined on the properties of modified CS. The grafting-to reaction was carried out in aqueous solution containing 4 vol% acetic acid, using ACVA as the radical initiator (Fig. 1). Thermal decomposition of ACVA generates radicals that can activate the thiocarbonylthio end group of the PCBMA macroCTA, producing PCBMA macroradicals. In parallel, radical sites may be generated on the deacetylated amino groups of CS. Similar radical-mediated grafting mechanisms have been previously proposed by Zaharia et al. [16], that grafted PNIPAAm onto the amine groups of CS via radical coupling. In our study, the formation of CS-g-PCBMA is proposed to occur through radical coupling between PCBMA macroradicals and chitosan radical sites associated with the amine groups, as shown in Fig. 1.

The ^{1}H NMR spectra of all studied CS-g-PCBMA copolymers are presented in Fig. S6a–c. The characteristic region of the ^{1}H NMR spectrum of CS-g-PCBMA$_{23}$ in D_2O containing 4 vol% acetic acid is shown in Fig. 2, together with the corresponding spectra of CS and PCBMA$_{23}$. For CS, the H2 proton of the glucosamine units (signal j) was observed at δ = ~3.06 ppm, while the remaining characteristic chitosan backbone signals assigned as k, l, and m appeared in the δ = ~3.8–3.5 ppm region. PCBMA$_{23}$ exhibited characteristic resonances at δ = 3.7 ppm (e), 3.58 – 3.45 ppm (g), 2.88 ppm (f), and 2.67 ppm (h), according to the assignments shown in Fig. 2. Signal f, assigned to the nitrogen-bound methyl groups of PCBMA, appeared at δ = 2.88 ppm [35]. The CS-g-PCBMA$_{23}$ spectrum contained characteristic signals originating from both the chitosan backbone and PCBMA grafts, including the chitosan signal j at δ = ~3.07 ppm and the PCBMA signal f at δ = ~2.87 ppm. The simultaneous presence of these characteristic resonances was used for the compositional analysis of the CS-g-PCBMA copolymers.

ATR-FTIR spectra of pristine chitosan, PCBMA$_{23}$ and CS-g-PCBMA$_{23}$ shown in Fig. 3 confirmed the presence of characteristic peaks associated with both chitosan and PCBMA$_{23}$ in the CS-g-PCBMA$_{23}$. The peaks at 1700 cm^{-1} and 1570 cm^{-1} correspond to the stretching vibrations of ester (−O–C=O) and carboxylate (−O–C=O$^-$) groups, while peak at 1150 cm^{-1} corresponds to the stretching vibrations of C–N [36] in PCBMA, whereas the peaks at 1670 cm^{-1} and 1010 cm^{-1} indicative of chitosan are assigned to carbonyl (–CO) and ether (−C–O–C) groups, respectively [37].

Based on ^{1}H NMR spectra and the molar mass values, degree of substitution (DS) and grafting density (GY) of each CS-g-PCBMA copolymer were calculated using equations (4) and (5) respectively (Table 1). For the longest grafts (DP 40), each chitosan chain was linked to on average 8 PCBMA side chains, corresponding to a substitution degree of 0.8% and a grafting yield of 31%. Reduction of PCBMA chain length to DP 23 caused the increase of the number of grafts to 21 per chitosan chain, raising the substitution degree to 2% and grafting yield to 49%. The shortest PCBMA chains (DP = 6) led to the highest grafting density with approximately 73 side chains per chitosan chain, substitution degree of 7% and grafting yield of 44%. The CS-g-PCBMA copolymers exhibited a clear inverse relationship between graft length and substitution density: shorter PCBMA chains attached more numerously to the chitosan backbone, whereas longer chains resulted in fewer but heavier grafts.

When compared with relevant data concerning grafted chitosan, the CS-g-PCBMA copolymers prepared in this study exhibited substitution degrees that were within the typical range observed for other grafted chitosan systems. These values were comparable to those reported by Dasgupta et al. [14] for PMEO$_2$MA (~3–12%), Ünlü et al. [38] for polyester grafts (~2–6%), and Lepoittevin et al. [18] for PHEMA–co–PF7 (up to ~10%). In some studies the grafting of chitosan was described as grafting percentage by mass; for PNIPAAm (Jiang et al. [17], Zaharia et al. [16], PAA (Hua et al. [15], Abbasian & Mahmoodzadeh [39], or mPEG–b–PAA grafts (Liu et al. [40], typical values ranged from 30% to 60%. These corresponded to relatively low site occupancies of approximately 1–3% when converted to substitution degree. Abbasi et al. [41] reported even lower substitution levels for PEG grafts, between ~0.24% and ~7%, depending on the chitosan molar mass. The substitution degrees obtained for CS-g-PCBMA are within the expected range for grafted chitosan derivatives reported in the literature.

4.2. Thin-film studies

The hydrophilic modification of chitosan chain would influence the copolymers' properties when placed on a planar surface. To correlate grafting density of CS-g-PCBMAs with their antifouling properties, thin-films were prepared via spin coating. They were initially measured by AFM to investigate film thickness and surface morphology, followed by contact angle measurement and protein antifouling studies. All results are shown in Table 2 and 3. In case of CS-g-PCBMA$_{40}$, homogeneous thin films could not be obtained as it did not fully dissolve under the applied conditions and instead produced large, visible gel-like particles.

4.2.1. AFM studies

AFM studies for pure CS films prepared from 5 and 10 mg/mL solutions shown in Fig. 4 and Fig. S7 and thickness, measured by surface scratch, was 36 nm and 90 nm, respectively. Film surfaces are smooth and homogeneous, with only sparse nanoscale features interrupting the flatness. Small brighter regions and occasional aggregates appeared, slightly more noticeable at the higher concentration. In any case, the overall morphology remained continuous and uniform, without signs of major roughness or phase separation. The CS surfaces exhibited sub-nanometer roughness, with estimated Rq values of approximately 0.8 nm for the 5 mg/mL solution film and 1.0 nm for the 10 mg/mL solution film.

The morphology of the CS-g-PCBMA$_{23}$ thin films is shown in Fig. 5 and Fig. S8, respectively for 5 mg/mL and 10 mg/mL concentration of

Table 1
Molecular characteristics of CS-g-PCBMA copolymers.

Sample	Chitosan M_n [Da]	PCBMA M_n [Da]	DP of PCBMA	Chitosan [wt%][**]	PCBMA [wt %][**]	PCBMA chains per CS chain (Eq. (1)	GY [%] (Eq. (5)	DS [%] (Eq. (4)
CS-g-PCBMA$_{40}$	164,000	9200*	40	70	30	8	31	0.8
CS-g-PCBMA$_{23}$	164,000	5200*	23	60	40	21	49	2
CS-g-PCBMA$_6$	164,000	1500*	6	60	40	73	44	7

* Calculated via SEC.
** Weight % in copolymer calculated via ^{1}H-NMR.

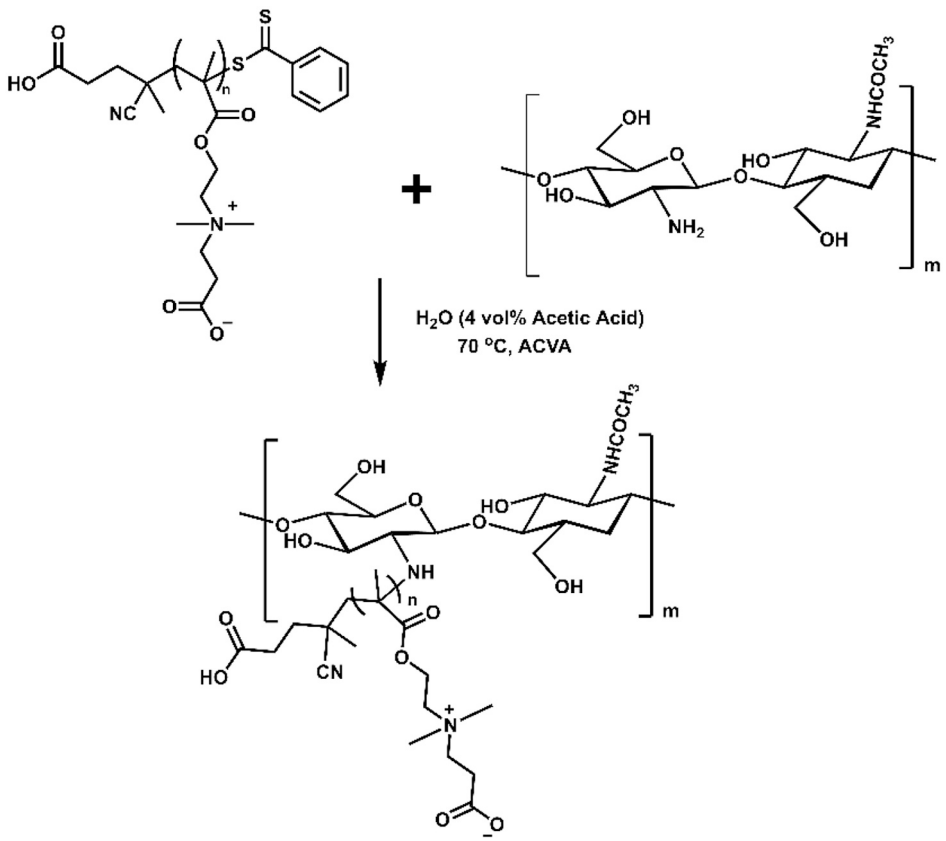


Fig. 1. Proposed reaction route of PCBMA grafting onto CS in water containing 4 vol% of acetic acid.

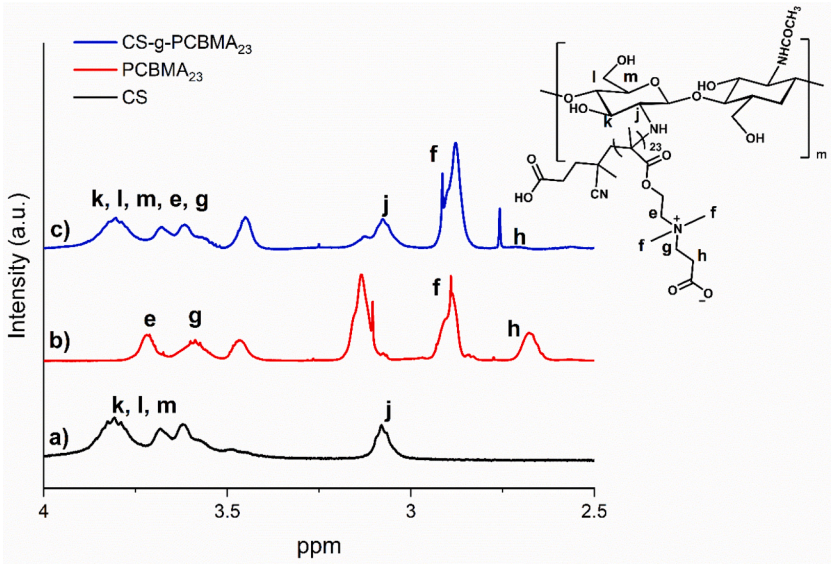


Fig. 2. Part of ^{1}H NMR spectra of (a) chitosan (b) $PCBMA_{23}$ and (c) chitosan-g-$PCBMA_{23}$ in D_2O (4 vol% acetic acid).

spin-coated solutions. For the CS-g-$PCBMA_{23}$ 5 mg/mL, AFM micrographs revealed a continuous and homogeneous film with a finely textured topography composed of nanoscale protrusions and shallow depressions distributed uniformly across the surface, with peak-to-valley differences within ±15 nm. The overall film thickness was 45 nm, measured by surface scratch, the root-mean-square (R_q) roughness of 2.37 nm and average roughness (R_a) of 1.92 nm.

The surface of CS-g-$PCBMA_{23}$ prepared from 10 mg/mL solution (Fig. S8) displayed a continuous and compact structure with a slightly more pronounced nanoscale texture compared to the thinner film. The 3D representation revealed rounded hill-like features and shallow depressions distributed uniformly across the surface, with height variations within ±15 nm. The film thickness was measured at 100 nm, with the root-mean-square (R_q) roughness of 3.39 nm, and average roughness (R_a) 2.81 nm.

Thin films of densely grafted CS-g-PCBMA6 copolymers prepared from 5 mg/mL solutions formed highly compact and homogeneous surfaces, as shown in Fig. 6. The thickness was 40 nm. The height

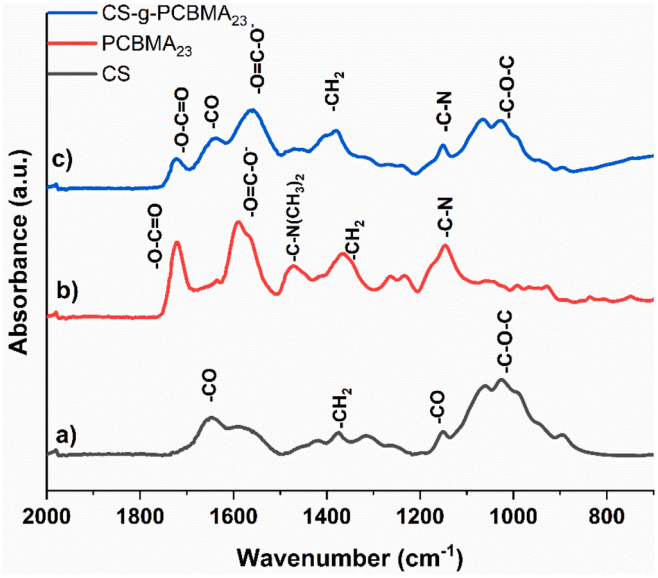


Fig. 3. ATR-FTIR spectra of (a) chitosan, (b) $PCBMA_{23}$ and (c) CS-g-$PCBMA_{23}$.

Table 2
Thin-film characteristics.

Sample	Solution concentration (mg/mL)	Film thickness (nm)	R_a (nm)	R_q (nm)
CS	5	36	0.64 ± 0.1	~0.80 ± 0.2
CS	10	90	0.81 ± 0.1	~1.00 ± 0.2
CS-g-$PCBMA_{23}$	5	45	1.92 ± 0.1	2.37 ± 0.2
CS-g-$PCBMA_{23}$	10	100	2.81 ± 0.3	3.39 ± 0.4
CS-g-$PCBMA_6$	5	40	0.46 ± 0.1	0.58 ± 0.2
CS-g-$PCBMA_6$	10	90	0.41 ± 0.2	0.52 ± 0.1

variation remained within ±20 nm, with R_q at 0.58 nm and R_a at 0.46 nm, indicating an exceptionally smooth coating. For 10 mg/mL solutions thickness increased to 90 nm (Fig. S9) and maintained a highly uniform, densely packed morphology without phase separation or particulate features. Both 2D and 3D images showed a narrow height variation of ±20 nm, while R_q and R_a were 0.52 and 0.41 nm, respectively.

The morphology of CS films studied here by AFM are similar to those reported in the literature. Garreau et al. [42] reported ultrasmooth chemically grafted chitosan films on silicon wafers, with RMS roughness values below 2 nm for thin spin-coated films. Similar nanoscale roughness values have also been reported for pristine chitosan films prepared by casting. Jakubowska et al. [43] reported R_q values of 1.1 ± 0.2 and 2.0 ± 0.2 nm for unmodified chitosan films with different degrees of deacetylation. A grafting-induced smoothing effect was reported for chitosan-g-PVP copolymers [44], where AFM showed that grafting reduced the rugged, scaly morphology of native chitosan and decreased the average roughness from 8.79 to 6.3 nm.

4.2.2. *SEM studies*

SEM imaging provided complementary information on the larger-scale morphology of all thin-film samples (Fig. 7 and Fig. S10). Both CS films exhibited continuous and generally smooth surfaces with sparse isolated particulate features. CS-g-$PCBMA_{23}$ coatings showed a more heterogeneous morphology, characterized by dispersed rounded surface features. CS-g-$PCBMA_6$ coatings displayed the most uniform and featureless surfaces among the investigated samples. No large-scale cracking or porous morphology was observed for any of the coatings at the investigated scale. These observations were consistent with the AFM results, which also indicated particularly smooth surfaces for the densely grafted CS-g-$PCBMA_6$ coatings.

4.2.3. *Contact angle studies*

Contact angle measurements of samples reflect the impact of both composition and film thickness (Fig. 8). The bare silicon-oxide wafer (Fig. 8a) showed a contact angle of ~44° ± 3, measured 1 h after plasma-cleaning.

CS films prepared from 5 mg/mL solutions exhibited a water contact angle of 51 ± 5°. CS films prepared from 10 mg/mL solutions showed a lower value of 38 ± 3°. The difference between the two preparation conditions indicates a change in the wettability of the resulting CS films. Increasing the polymer concentration resulted in an increase in film thickness from approximately 36 to 90 nm and may have influenced film formation, surface organization, and morphology. The measured contact-angle values remain within the range previously reported for chitosan-based thin films [42,45]. Garreau et al. [42] reported values around 62° for spin-coated chitosan on silicon, while Lee et al. [45] observed a broader range of contact angles ~40–70° depending on preparation and blending with other components.

Thin films prepared from 5 mg/mL CS-g-$PCBMA_{23}$ solutions displayed a contact angle of ~10 ± 2°, while for 10 mg/mL solutions of 18

Table 3
Characteristics of CS and CS-g-PCBMA thin films and their behavior towards BSA.

Sample Type	Concentration (mg/mL)	Thin film thickness (nm)[a]	Contact Angle	BSA retention (μg/cm²)[b]	Relative BSA retention % of CS prepared from 5 mg/mL	BSA retention reduction % vs CS prepared from 5 mg/mL
wafer	–	–	44 ± 3°	bdl	0	100
CS	5	36	51 ± 5°	156	100	0
CS	10	90	38 ± 3°	146	94	6
CS-g-$PCBMA_{23}$	5	45	10 ± 2°	90	58	42
CS-g-$PCBMA_{23}$	10	100	18 ± 3°	132	85	15
CS-g-$PCBMA_6$	5	40	17 ± 4°	120	77	23
CS-g-$PCBMA_6$	10	90	8 ± 2°	bdl	0	100

bdl: below detection limit.
For samples with BSA retention below the detection limit, relative retention and reduction were reported as 0% and 100%, respectively, within the sensitivity of the assay.
[a] Measured by AFM.
[b] Measured by UV–Vis and calculated via Eqs. (7) and (8).

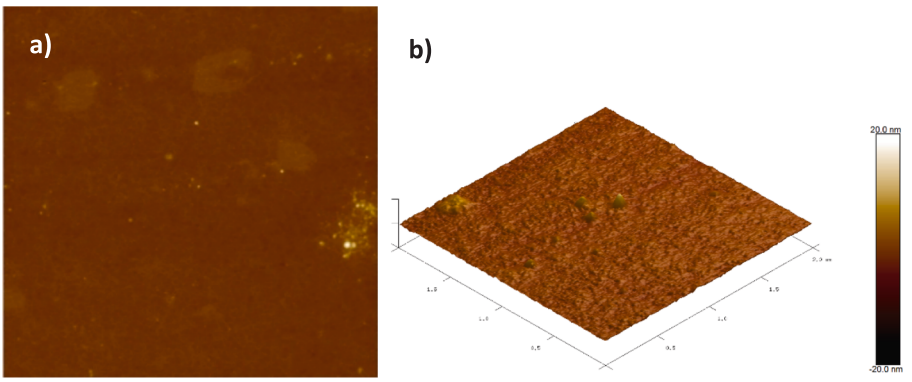


Fig. 4. (a) two-dimensional and (b) three-dimensional AFM images of CS thin films prepared from 5 mg/mL solutions (scale: 2 × 2 um).

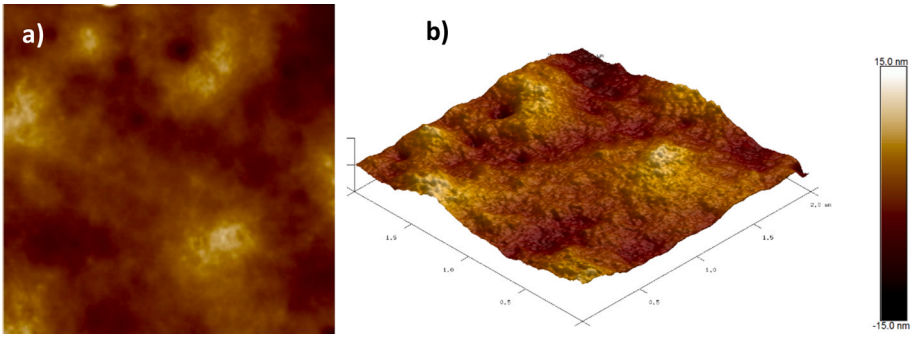


Fig. 5. (a) two-dimensional and (b) three-dimensional AFM images of CS-g-PCBMA$_{23}$ prepared from 5 mg/mL solution (scale: 2 × 2 um).

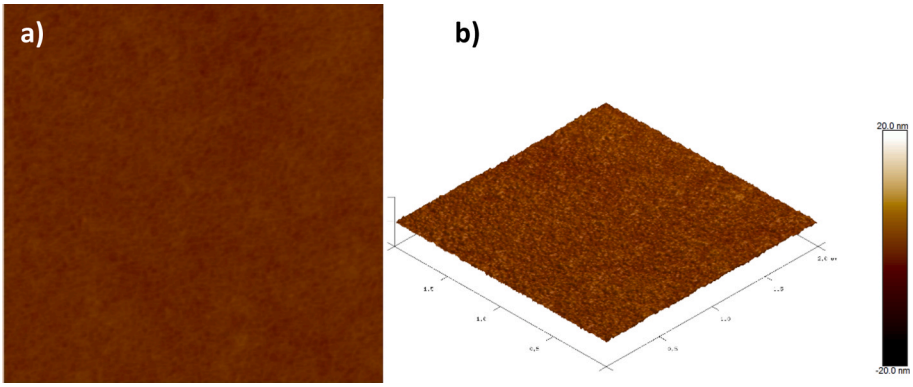


Fig. 6. (a) two-dimensional and (b) three-dimensional AFM images of CS-g-Pcbma$_6$ prepared from 5 mg/mL solutions (scale: 2 × 2 um).

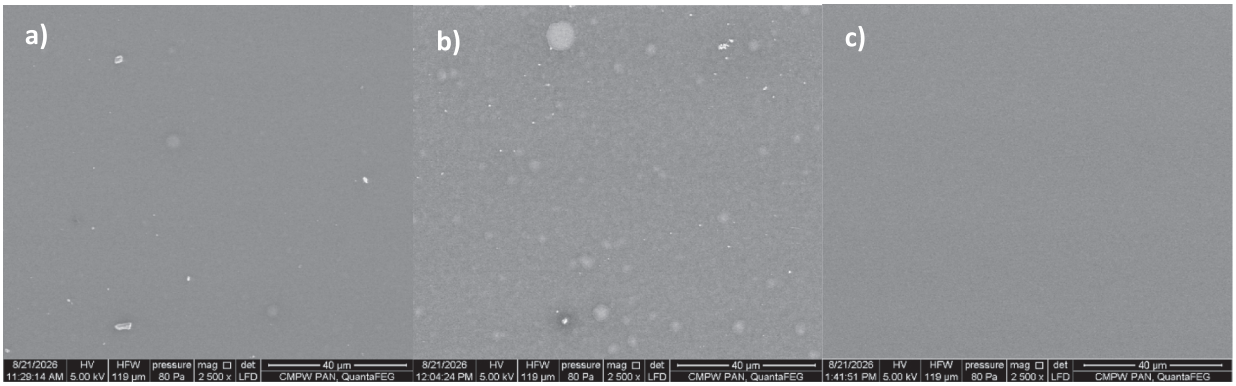


Fig. 7. SEM images of (a) CS (5 mg/mL, thickness 36 nm), (b) CS-g-PCBMA$_{23}$ (5 mg/mL, thickness 45 nm) and (c) CS-g-PCBMA$_6$ (5 mg/mL, thickness 40 nm).

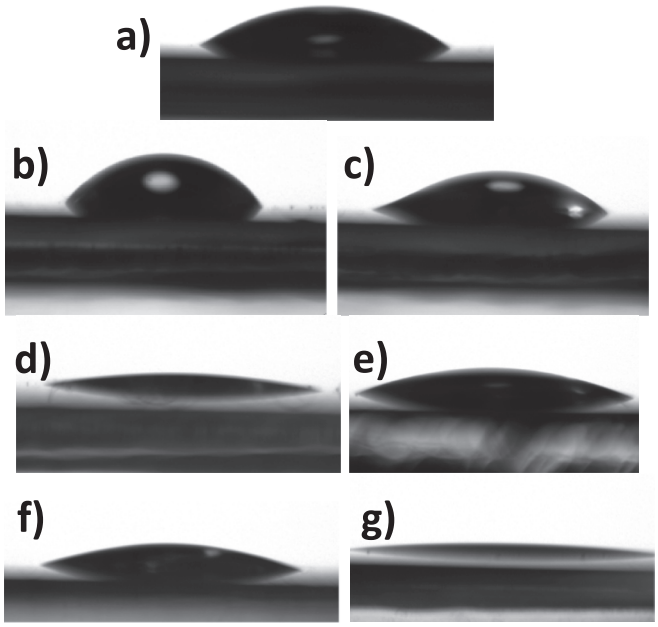


Fig. 8. Contact angle photos of (a) plasma-cleaned silicon oxide wafer, (b) CS (5 mg/mL, thickness 36 nm), (c) CS (10 mg/mL, thickness 90 nm), (d) CS-g-PCBMA$_{23}$ (5 mg/mL, thickness 45 nm), (e) CS-g-PCBMA$_{23}$ (10 mg/mL, thickness 100 nm), f) CS-g-PCBMA$_6$ (5 mg/mL, thickness 40 nm), (g) CS-g-PCBMA$_6$ (10 mg/mL, thickness 90 nm).

$\pm$ 3°. These low angles indicate extremely high hydrophilicity and indicate increased wettability compared to CS.

CS-g-PCBMA$_6$ thin films prepared from 5 and 10 mg/mL solutions exhibited contact angles of 17 $\pm$ 4° and 8 $\pm$ 2°, respectively, as shown in Fig. 8f and Fig. 8g. These values indicate highly wettable surfaces of superhydrophilic behavior. The very low contact angle indicates a highly wettable surface and is consistent with the strong hydrophilic character introduced by the PCBMA-containing coating.

4.2.4. *Protein fouling studies*

The protein fouling behavior of CS and CS-g-PCBMA thin-film coatings was evaluated using BSA as a model protein and the results are summarized in Table 3. In this work, BSA retention refers to the amount of BSA that remained associated with the thin films after washing, normalized to the exposed coating area, using a combination of eq. (7) and (8). The relative BSA retention put in the column of Table 3 expresses each value as a percentage of the CS film prepared from the 5 mg/mL solution. The final column of Table 3, BSA retention reduction vs CS, shows the percentage decrease in BSA retention compared with the CS film prepared from the 5 mg/mL solution. Pristine CS films were used as the reference coatings and the bare silicon oxide wafer served as a substrate control.

Pure CS thin films showed the highest BSA retention. This behavior reflects the known ability of chitosan to interact with proteins through electrostatic interactions, hydrogen bonding, and polymer-protein complexation [46–48].

PCBMA grafting was associated with reduced BSA retention relative to pristine CS under the investigated conditions. The CS-g-PCBMA$_{23}$ film prepared from the 5 mg/mL solution showed a relative BSA retention of 58%, corresponding to a 42% reduction compared with the CS reference. A weaker reduction of 15% compared to pure CS surface was measured for the thicker CS-g-PCBMA$_{23}$ film (100 nm) prepared from 10 mg/mL solution indicates that the protein-retention behavior was affected not only by chemical composition, but also by film thickness and surface morphology (Fig.S8).

The film prepared from 5 mg/mL solution of CS-g-PCBMA$_6$ showed 77% relative BSA retention, corresponding to a 23% reduction compared with the CS reference. The strongest antifouling effect was observed for CS-g-PCBMA$_6$ thin films prepared from the 10 mg/mL solution, where BSA retention was below the detection limit. This corresponds to almost complete reduction within the sensitivity of the assay and identifies this coating as the most protein-resistant sample in this study. This result is consistent with high grafting density of copolymer chains, very low water contact angle of 8°, and smooth AFM and SEM morphology (Fig. S9 and S10).

The reduced BSA retention observed for CS-g-PCBMA films was also observed for other modified chitosan-based antifouling coatings. Sun et al [19] showed that PCBMA brushes on CS nanofibers strongly suppressed nonspecific cell adhesion, while CS membranes modified with sulfobetaine-containing grafts showed reduced bacterial and blood-cell attachment [49,50]. CS-based hydrogel coatings containing poly(glycidyl methacrylate) and zwitterionic poly(phosphorylcholine) have also shown strong protein-fouling resistance, reducing the adsorption of fibrinogen, immunoglobulin, and lysozyme by approximately 90% compared with unmodified polyethylene [51]. Other chitosan-based systems with grafted chains, including CS/AgNP-grafted membranes [52], PEGylated chitosan coatings [53] and multilayers of ionic derivatives of chitosan [54] have also demonstrated improved resistance to bacterial adhesion, biofilm formation, and membrane biofouling.

5. Conclusions

Three PCBMA homopolymers with different chain lengths synthesized by RAFT polymerization were grafted onto chitosan through a proposed radical-coupling mechanism, producing copolymers with distinct grafting densities. The PCBMA chains had degrees of polymerization of 40, 23, and 6, corresponding to molar masses of 9200, 5200, and 1500 Da, respectively. Shorter PCBMA chains were grafted densely onto the chitosan backbone, while longer chains showed lower incorporation due to steric hindrance during the grafting-to reaction.

CS and CS-g-PCBMA copolymers were deposited as model thin films on silicon oxide wafers by spin coating. The films were examined to observe how PCBMA grafting affected surface morphology, wettability, and BSA retention. CS-g-PCBMA$_6$ formed the smoothest and most homogeneous films, as shown by AFM. These films also showed the strongest increase in wettability, compared to the others, reaching a water contact angle of 8° for the coating prepared from the 10 mg/mL solution. This indicated that dense grafting of short PCBMA chains on chitosan backbone allows to produce superhydrophilic coating on silicon oxide wafer.

The BSA retention results showed that pure CS films retained protein, whereas surfaces coated with PCBMA-grafted CS exhibited improved resistance to protein fouling. The influence of grafting density was most evident for CS-g-PCBMA$_6$ prepared from the 10 mg/mL solution, for which BSA retention was below the detection limit.

This work demonstrated how PCBMA chain length and grafting density can control the surface behavior of CS-g-PCBMA thin films. Dense grafting with short PCBMA chains produced smooth, highly wettable, and protein-resistant chitosan-based coatings. These findings provide a simple strategy for designing zwitterionic chitosan materials with improved hydration and antifouling properties.

CRediT authorship contribution statement

Theodore Sentoukas: Writing – review & editing, Writing – original draft, Software, Methodology, Investigation, Formal analysis, Data curation, Conceptualization. **Andrzej Marcinkowski:** Software, Investigation. **Wojciech Wałach:** Writing – review & editing. **Karolina Olszowska:** Methodology. **Aristeidis Papagiannopoulos:** Writing – review & editing, Conceptualization. **Stergios Pispas:** Writing – review

& editing, Conceptualization. **Barbara Trzebicka:** Writing – review & editing, Supervision, Conceptualization.

Declaration of competing interest

The authors declare that they have no known competing financial interests or personal relationships that could have appeared to influence the work reported in this paper.

Appendix A. Supplementary material

Supplementary data to this article can be found online at https://doi.org/10.1016/j.apsusc.2026.168516.

Data availability

Data will be made available on request.

References

[1] Y. Herdiana, E. Febrina, S. Nurhasanah, D. Gozali, K.M. Elamin, N. Wathoni, Drug loading in chitosan-based nanoparticles, Pharmaceutics 16 (2024) 1043, https://doi.org/10.3390/pharmaceutics16081043.

[2] H. Yadav, R. Malviya, N. Kaushik, Chitosan in biomedicine: a comprehensive review of recent developments, Carbohydr. Polym. Technol. Appl. 8 (2024) 100551, https://doi.org/10.1016/j.carpta.2024.100551.

[3] A. Stefanache, I.I. Lungu, N. Anton, D. Damir, C. Gutu, I. Olaru, A. Plesea Condratovici, M. Duceac (Covrig), M. Constantin, G. Calin, et al., Chitosan Nanoparticle-based drug delivery systems: advances, challenges, and future perspectives, Polymers 17 (2025) 1453, https://doi.org/10.3390/polym17111453.

[4] G. Kumar, T. Virmani, S.K. Misra, A. Sharma, K. Pathak, Exploration of chitosan and its modified derivatives as vaccine adjuvant: a review, Carbohydr. Polym. Technol. Appl. 8 (2024) 100537, https://doi.org/10.1016/j.carpta.2024.100537.

[5] S. Li, W. Pan, M. Zhang, K. Song, Z. Zhou, Q. Zhao, G.-Z. Li, C. Zhu, Chitosan-based dressing materials for burn wound healing, Polymers 17 (2025) 1647, https://doi.org/10.3390/polym17121647.

[6] D. Ianev, B. Vigani, C. Valentino, M. Sorrenti, L. Catenacci, M.C. Bonferoni, M. Ruggeri, G. Sandri, M. Mori, S. Rossi, Whey protein-chitosans complexes as sustainable and value-added biomaterials for wound healing, Carbohydr. Polym. Technol. Appl. 9 (2025) 100643, https://doi.org/10.1016/j.carpta.2024.100643.

[7] K. Khodaverdi, S.M. Naghib, M.R. Mozafari, M. Rahmanian, Chitosan/Hydroxyapatite hydrogels for localized drug delivery and tissue engineering: a review, Carbohydr. Polym. Technol. Appl. 9 (2025) 100640, https://doi.org/10.1016/j.carpta.2024.100640.

[8] P.O. Boamah, J. Onumah, T. Salifu, J.H. Essel, B. Apam, Removal of lithium onto chitosan derivative using taguchi method, Carbohydr. Polym. Technol. Appl. 8 (2024) 100611, https://doi.org/10.1016/j.carpta.2024.100611.

[9] M.Z. Elsabee, E.S. Abdou, Chitosan based edible films and coatings: a review, Mater. Sci. Eng. C 33 (2013) 1819–1841, https://doi.org/10.1016/j.msec.2013.01.010.

[10] G. Kerch, Chitosan films and coatings prevent losses of fresh fruit nutritional quality: a review, Trends Food Sci. Technol. 46 (2015) 159–166, https://doi.org/10.1016/j.tifs.2015.10.010.

[11] M. Rinaudo, Chitin and chitosan: properties and applications, Prog. Polym. Sci. 31 (2006) 603–632, https://doi.org/10.1016/j.progpolymsci.2006.06.001.

[12] D. Kumar, S. Gihar, M.K. Shrivash, P. Kumar, P.P. Kundu, A Review on the synthesis of graft copolymers of chitosan and their potential applications, Int. J. Biol. Macromol. 163 (2020) 2097–2112, https://doi.org/10.1016/j.ijbiomac.2020.09.060.

[13] V.K. Thakur, M.K. Thakur, Recent advances in graft copolymerization and applications of chitosan: a review, ACS Sustain. Chem. Eng. 2 (2014) 2637–2652, https://doi.org/10.1021/sc500634p.

[14] N. Dasgupta, D. Sun, M. Gorbet, M. Gauthier, Chitosan grafted with thermoresponsive poly(di(ethylene glycol) methyl ether methacrylate) for cell culture applications, Polymers 15 (2023) 1515, https://doi.org/10.3390/polym15061515.

[15] D. Hua, J. Tang, J. Cheng, W. Deng, X. Zhu, A novel method of controlled grafting modification of chitosan via RAFT polymerization using chitosan-RAFT agent, Carbohydr. Polym. 73 (2008) 98–104, https://doi.org/10.1016/j.carbpol.2007.11.008.

[16] M.-M. Zaharia, F. Bucatariu, M. Karayianni, E.-D. Lotos, M. Mihai, S. Pispas, Synthesis of thermoresponsive chitosan-graft-Poly(N-isopropylacrylamide) hybrid copolymer and its complexation with DNA, Polymers 16 (2024) 1315, https://doi.org/10.3390/polym16101315.

[17] J. Jiang, X. Pan, J. Cao, J. Jiang, D. Hua, X. Zhu, Synthesis and property of chitosan graft copolymer by RAFT polymerization with tosylic acid–chitosan complex, Int. J. Biol. Macromol. 50 (2012) 586–590, https://doi.org/10.1016/j.ijbiomac.2012.01.033.

[18] B. Lepoittevin, T. Elzein, D. Dragoe, A. Bejjani, F. Lemée, J. Levillain, P. Bazin, P. Roger, I. Dez, Hydrophobization of chitosan films by surface grafting with fluorinated polymer brushes, Carbohydr. Polym. 205 (2019) 437–446, https://doi.org/10.1016/j.carbpol.2018.10.044.

[19] N. Sun, M. Liu, J. Wang, Z. Wang, X. Li, B. Jiang, R. Pei, Chitosan nanofibers for specific capture and nondestructive release of CTCs assisted by pCBMA brushes, Small 12 (2016) 5090–5097, https://doi.org/10.1002/smll.201600475.

[20] J.C. Hower, M.T. Bernards, S. Chen, H.-K. Tsao, Y.-J. Sheng, S. Jiang, Hydration of "Nonfouling" functional groups, J. Phys. Chem. B 113 (2009) 197–201, https://doi.org/10.1021/jp8065713.

[21] S. Chen, L. Li, C. Zhao, J. Zheng, Surface hydration: principles and applications toward low-fouling/nonfouling biomaterials, Polymer 51 (2010) 5283–5293, https://doi.org/10.1016/j.polymer.2010.08.022.

[22] L.D. Blackman, P.A. Gunatillake, P. Cass, K.E.S. Locock, An introduction to zwitterionic polymer behavior and applications in solution and at surfaces, Chem. Soc. Rev. 48 (2019) 757–770, https://doi.org/10.1039/C8CS00508G.

[23] C.R. Emmenegger, E. Brynda, T. Riedel, Z. Sedlakova, M. Houska, A.B. Alles, Interaction of blood plasma with antifouling surfaces, Langmuir 25 (2009) 6328–6333, https://doi.org/10.1021/la900083s.

[24] F. Ding, S. Yang, Z. Gao, J. Guo, P. Zhang, X. Qiu, Q. Li, M. Dong, J. Hao, Q. Yu, et al., Antifouling and pH-responsive poly(carboxybetaine)-based nanoparticles for tumor cell targeting, Front. Chem. 7 (2019) doi:10.3389/fchem.2019.00770.

[25] G. Ma, F. Ji, W. Lin, S. Chen, Determination of non-freezing water in different nonfouling materials by differential scanning calorimetry, J. Biomater. Sci. Polym. Ed. 33 (2022) 1012–1024, https://doi.org/10.1080/09205063.2022.2034285.

[26] H. Zhu, L. Li, J. Shen, Molecular dynamics simulations suggest conformational and hydration difference between zwitterionic poly (carboxybetaine methacrylate) and poly (ethylene glycol), Chem. Phys. 532 (2020), https://doi.org/10.1016/j.chemphys.2019.110599.

[27] G. Zhao, X. Dong, Y. Sun, Self-assembled curcumin-poly(carboxybetaine methacrylate) conjugates: potent nano-inhibitors against amyloid β-protein fibrillogenesis and cytotoxicity, Langmuir 35 (2019) 1846–1857, https://doi.org/10.1021/acs.langmuir.8b01921.

[28] G. Zhao, F. Qi, X. Dong, J. Zheng, Y. Sun, LVFFARK conjugation to poly (carboxybetaine methacrylate) remarkably enhances its inhibitory potency on amyloid β-protein fibrillogenesis, React. Funct. Polym. 140 (2019) 72–81, https://doi.org/10.1016/j.reactfunctpolym.2019.04.003.

[29] W. Yang, S. Liu, T. Bai, A.J. Keefe, L. Zhang, J.R. Ella-Menye, Y. Li, S. Jiang, Poly (carboxybetaine) nanomaterials enable long circulation and prevent polymer-specific antibody production, Nano Today 9 (2014) 10–16, https://doi.org/10.1016/j.nantod.2014.02.004.

[30] X. Song, J. Man, X. Zhang, J. Wang, Y. Zhang, J. Li, J. Du, Y. Chen, J. Li, Y. Chen, Atomistic insights into the ionic response and mechanism of antifouling zwitterionic polymer brushes, Small 21 (2025) 2406233, https://doi.org/10.1002/smll.202406233.

[31] Y. Liu, D. Zhang, B. Ren, X. Gong, L. Xu, Z.-Q. Feng, Y. Chang, Y. He, J. Zheng, Molecular simulations and understanding of antifouling zwitterionic polymer brushes, J. Mater. Chem. B 8 (2020) 3814–3828, https://doi.org/10.1039/d0tb00520g.

[32] D.J. Liaw, C.C. Huang, W.F. Lee, J. Borbély, E.T. Kang, Synthesis and characteristics of the poly(carboxybetaine)s and the corresponding cationic polymers, J. Polym. Sci., Part A:Polym. Chem. 35 (1997) 3527–3536, https://doi.org/10.1002/(SICI)1099-0518(19971130)35:16<3527::AID-POLA19>3.0.CO;2-H.

[33] H. Massoumi, M.K. Chug, G.H. Nguyen, E.J. Brisbois, A multidisciplinary experiment to characterize antifouling biocompatible interfaces via quantification of surface protein adsorption, J. Chem. Educ. 99 (2022) 2667–2676, https://doi.org/10.1021/acs.jchemed.2c00208.

[34] V. Hlady, J. Buijs, H.P. Jennissen, Methods for studying protein adsorption, in: Methods in Enzymology, Elsevier, 1999, pp. 402–429. ISBN 978-0-12-182210-1.

[35] H. Peng, W. Ji, R. Zhao, Z. Lu, J. Yang, Y. Li, X. Zhang, PH-sensitive zwitterionic polycarboxybetaine as a potential non-viral vector for small interfering RNA delivery, RSC Adv. 10 (2020) 45059–45066, https://doi.org/10.1039/d0ra09359a.

[36] B. Smith, The carbonyl functional group, in: Infrared Spectral Interpretation, 2018, pp. 91–124. ISBN 978-0-203-75084-1.

[37] B. Smith, Functional groups containing the C-O bond, in: Infrared Spectral Interpretation, 2018, pp. 67–90. ISBN 978-0-203-75084-1.

[38] C.H. Ünlü, E. Pollet, L. Avérous, Original Macromolecular Architectures based on Poly(ε-Caprolactone) and Poly(ε-Thiocaprolactone) Grafted onto Chitosan Backbone, Int. J. Mol. Sci. 19 (2018) 3799, https://doi.org/10.3390/ijms19123799.

[39] M. Abbasian, F. Mahmoodzadeh, Synthesis of antibacterial silver–chitosan-modified bionanocomposites by RAFT polymerization and chemical reduction methods, J. Elastomers Plast. 49 (2017) 173–193, https://doi.org/10.1177/0095244316644858.

[40] C. Liu, X. Wang, R. Liu, Y. Wu, S. Luo, A new multifunctional polymer: synthesis and characterization of mPEG-b-PAA-grafted chitosan copolymer, J. Cent. South Univ. Technol. 17 (2010) 936–942, https://doi.org/10.1007/s11771-010-0580-7.

[41] S. Abbasi, G. Yousefi, O. Firuzi, S. Mohammadi-Samani, Design and cell cytotoxicity assessment of palmitoylated polyethylene glycol-grafted chitosan as nanomicelle carrier for paclitaxel, J. Appl. Polym. Sci. 133 (2016), https://doi.org/10.1002/app.43233.

[42] C. Garreau, L. Chiappisi, S. Micciulla, I. Morfin, S. Trombotto, T. Delair, G. Sudre, Preparation of highly stable and ultrasmooth chemically grafted thin films of chitosan, Soft Matter 19 (2023) 1606–1616, https://doi.org/10.1039/D3SM00003F.

[43] E. Jakubowska, M. Gierszewska, J. Nowaczyk, E. Olewnik-Kruszkowska, Physicochemical and storage properties of chitosan-based films plasticized with deep eutectic solvent, Food Hydrocoll. 108 (2020) 106007, https://doi.org/10.1016/j.foodhyd.2020.106007.
[44] M.S. Lavlinskaya, A.V. Sorokin, A.A. Mikhaylova, E.I. Kuznetsov, D. R. Baidamshina, I.A. Saranov, M.V. Grechkina, M.G. Holyavka, Y.F. Zuev, A. R. Kayumov, et al., The low-waste grafting copolymerization modification of chitosan is a promising approach to obtaining materials for food applications, Polymers 16 (2024) 1596, https://doi.org/10.3390/polym16111596.
[45] J.H. Lee, T. Tachibana, H. Wadamori, K. Yamana, R. Kawasaki, S. Kawamura, H. Isozaki, M. Sakuragi, I. Akiba, A. Yabuki, Drug-loaded biocompatible chitosan polymeric films with both stretchability and controlled release for drug delivery, ACS Omega 8 (2023) 1282–1290, https://doi.org/10.1021/acsomega.2c06719.
[46] V. Boeris, B. Farruggia, G. Picó, Chitosan–bovine serum albumin complex formation: a model to design an enzyme isolation method by polyelectrolyte precipitation, J. Chromatogr. B: Anal. Technol. Biomed Life Sci. 878 (2010) 1543–1548, https://doi.org/10.1016/j.jchromb.2010.04.008.
[47] Y. Xie, J. Ding, Y. Li, P. Wei, S. Liu, R. Yang, The formation of protein–chitosan complexes: their interaction, applications, and challenges, Foods 13 (2024) 3572, https://doi.org/10.3390/foods13223572.
[48] L.S. Estevam, H.S. Debone, C.M.P. Yoshida, C.F. Da Silva, Adsorption of bovine serum and bovine haemoglobin onto chitosan film, Adsorpt. Sci. Technol. 30 (2012) 785–792, https://doi.org/10.1260/0263-6174.30.8-9.785.
[49] X. Zhai, B. Chen, Y. He, L. An, S. Chen, X. Yan, Y. Zhang, J. Meng, A novel loose nanofiltration membrane with superior anti-biofouling performance prepared from zwitterion-grafted chitosan, J. Taiwan Inst. Chem. Eng. 132 (2022) 104191, https://doi.org/10.1016/j.jtice.2021.104191.
[50] H.-T. Lin, A. Venault, Y. Chang, Zwitterionized chitosan based soft membranes for diabetic wound healing, J. Membr. Sci. 591 (2019) 117319, https://doi.org/10.1016/j.memsci.2019.117319.
[51] J. Xv, H. Li, W. Zhang, G. Lai, H. Xue, J. Zhao, M. Tu, R. Zeng, Anti-biofouling and functionalizable bioinspired chitosan-based hydrogel coating via surface photo-immobilization, J. Biomater. Sci. Polym. Ed. 30 (2019) 398–414, https://doi.org/10.1080/09205063.2019.1570435.
[52] Q.X. Duong, N.H. Do, H.T. Pham, T.H.A. Ngo, The enhancement of antibacterial and anti-biofouling properties of chitosan/silver nanoparticles-grafted composite polyamide membrane, J. of Applied Polymer Sci. 140 (2023) e54440, https://doi.org/10.1002/app.54440.
[53] D. Yu, F. Ye, S. Dobretsov, J. Dutta, Antifouling activity of PEGylated chitosan coatings: impacts of the side chain length and encapsulated ZnO/Ag nanoparticles, Int. J. Biol. Macromol. 281 (2024) 136316, https://doi.org/10.1016/j.ijbiomac.2024.136316.
[54] M. Bulwan, K. Wójcik, S. Zapotoczny, M. Nowakowska, Chitosan-based ultrathin films as antifouling, anticoagulant and antibacterial protective coatings, J. Biomater. Sci. Polym. Ed. 23 (2012) 1963–1980, https://doi.org/10.1163/092050611X601711.